AIAA JOURNAL
Vol. 35, No. 3, March 1997

Multigrid Acceleration of a High-Resolution Computational Aeroacoustics Scheme

Yusuf Özyörük* and Lyle N. Long†
Pennsylvania State University, University Park, Pennsylvania 16802-1401

A multigrid method is applied to a fourth-order accurate (spatially and temporally) finite difference Runge–Kutta time-marching scheme. This is used to solve the nonlinear Euler equations for the efficient prediction of noise radiation from turbofan engine inlets. This noise prediction approach computes a steady-state solution first, and then a source is turned on and the unsteady solution is computed. This has the advantage of using the same numerical scheme to evaluate the residuals of the governing equations in both the steady and unsteady calculations, which means that the steady-state solution is smooth and no numerical errors contaminate the acoustic solution. The high-resolution steady-state flowfields are calculated efficiently using a full approximation storage multigrid method. This makes it to possible to attain steady-state solutions on extremely fine meshes designed for high-frequency turbofan noise problems. It is also shown that acoustic results for a JT15D inlet are accurately represented by the present approach.

I. Introduction

THE emergence of powerful parallel computers has recently made the inclusion of more physics in the numerical simulations of aeroacoustic problems[1,2] possible by solving the full Euler or Navier–Stokes equations. In this approach, however, the acoustic field is obtained by taking the difference between the instantaneous and mean flowfields. If the transient part of the instantaneous pressure is associated only with acoustic waves, the mean field will be equivalent to a solution that will be obtained with the application of time-invariant boundary conditions (BC) in the near field (e.g., steady solid wall BC). This solution is often referred to as the steady-state solution. An example case where the transient flowfield is driven only by acoustic waves is a turbofan engine inlet at steady flight.

A hybrid, nonlinear, parallel, time-domain code[2–4] has been developed as part of an ongoing research effort to predict ducted fan noise. This code solves the three-dimensional Euler equations to determine the near-field acoustics and uses a moving surface Kirchhoff formula[5] to predict the far-field noise. The flow solver uses an explicit, spatially and temporally fourth-order accurate, finite difference, Runge–Kutta (R–K) time-integration scheme. Because of the approach taken, the steady-state solution is obtained first and then the time-accurate inlet fan-face conditions (acoustic sources) are turned on, and the solution is advanced in a time-accurate manner. This procedure inherently requires that the same scheme, namely fourth-order central finite difference, be used to evaluate the residuals of the governing equations in both the steady and time-accurate calculations so that starting from the steady solution is smooth and no spurious waves are generated.

However, there are several difficulties associated with using a high-order explicit scheme for steady-state calculations. The fourth-order scheme is really designed for time-accurate problems with low dissipation and dispersion. In other words, low-frequency modes are not damped out. Moreover, typical turbofan inlet radiation problems involve high blade-passing frequencies (BPF). Hence, very fine meshes are usually needed, resulting in very small time steps and consequently slow convergence. Also, turbofan noise predictions are often made at low freestream Mach numbers as associated with landing or takeoff conditions, which are considered more critical in terms of community noise regulations. The disparity of the eigenvalues in these cases is a degrading factor in achieving sufficiently rapid steady-state solutions.

Though some of these difficulties can be avoided by a totally different approach, such as that using nonlinear disturbance equations,[6] where the mean field could be found by an efficient flow solver, there are several convergence acceleration procedures that can be applied to full, explicit, Euler/Navier–Stokes solvers. Because it is important here to preserve the discretized form of the residuals of the governing equations in both the steady and unsteady calculations, the full approximation storage (FAS) multigrid scheme of Jameson[7] serves as an appropriate tool for efficient steady-state flow computations. This multigrid method has been widely used in the computational fluid dynamics community[8–10] for pseudo-time marching of the time-dependent Euler/Navier–Stokes equations. However, to the authors' knowledge, this use has remained limited only to second-order algorithms (finite volume or finite difference). Several other high-order multigrid implementations appeared only together with implicit (matrix inversion) schemes.[11,12] In this paper, the FAS multigrid technique is extended to our hybrid, parallel computational aeroacoustics (CAA) method[2–4] retaining its fourth-order spatial accuracy.

This extension is described later, and results showing the convergence improvements for steady-state flow calculations around the JT15D engine inlet are presented. It is also demonstrated by some unsteady inlet problems that starting the time-accurate solution process from the multigrid solution does not cause any spurious wave developments and the resultant acoustic fields are accurately represented by the present approach.

II. Ducted Fan Noise Code

The hybrid ducted fan noise radiation code[2–4] solves the three-dimensional Euler equations on a three-dimensional, body-fitted coordinate system and passes the near-field acoustic pressure to a Kirchhoff method based on the formulation of Farassat and Myers[5] to predict the far-field sound. The governing equations are solved in a relatively small domain using nonreflecting BC based on the work of Bayliss and Turkel[13] and Tam and Webb.[14] An orthogonal mesh system is created through a sequence of conformal mappings,[3,15] and the governing equations are formulated in cylindrical coordinates to effectively treat the grid singularity at the centerline. Fourth-order accurate, cell-centered finite differencing and four-stage, noncompact R–K time integration are performed to advance the solution. Adaptive artificial dissipation[16,17] is used to suppress spurious waves. The acoustic source is formed using the eigensolutions of the cylindrical duct problem and the rotor–stator interaction theory of Tyler and Sofrin.[18] The Euler solver and the Kirchhoff

Received Feb. 21, 1996; revision received Sept. 30, 1996; accepted for publication Oct. 27, 1996; also published in *AIAA Journal on Disc*, Volume 2, Number 2.

*Postdoctoral Scholar, Department of Aerospace Engineering. Member AIAA.

†Associate Professor, Department of Aerospace Engineering. Senior Member AIAA.

method are coupled such that as soon as the Euler solution becomes available, the Kirchhoff surface integrations are performed in a forward time-binning manner to predict the far-field noise. All calculations are carried out on parallel computers using the data parallel paradigm. Özyörük and Long[4] describe the fourth-order flow solver with emphasis on the hybrid code's parallel aspects. Özyörük and Long[2] discuss the acoustic source model and the Kirchhoff coupling issues for engine inlet noise predictions.

III. Multigrid Method

Through a multigrid method, low-frequency errors of the fine grid solution are transferred onto a sequence of coarse grids and are smoothed by updating the solution. Then the corrections to the solution obtained on the coarse grids are interpolated back to the fine grid with its own low-frequency errors having been aliased into high-frequency errors that can now be damped out on the fine mesh.

This procedure is applied in a systematic way to push the low-frequency errors quickly out of the domain. Hence, a significant convergence improvement is gained, basically for two reasons.[9,19] First, the number of operations required for each iteration to update the solution is reduced significantly on coarse grids because of fewer grid points. Second, the time step sizes on coarse grids are larger than on the fine grid. In other words, the effect of the BC that drive the flowfield is felt more rapidly throughout the domain.

In multigrid methods the grids of varying coarseness are usually obtained by simply deleting every other grid line of the next finer grid. The fine grid size (number of grid points) is chosen such that the grid lines representing the boundaries are retained in this process.

A. FAS Scheme

The semidiscretized Euler equations and the far-field BC[3,4] are all written as

$$\frac{\mathrm{d}\boldsymbol{Q}}{\mathrm{d}t} = -J\,[\mathcal{F}(\boldsymbol{Q}) - \mathcal{D}(\boldsymbol{Q})] \tag{1}$$

where $\boldsymbol{Q}$ is the vector of dependent solution variables (conservative state variables for the interior points, perturbations of primitive variables for the outer boundaries), J is the Jacobian of the coordinate transformation, $\mathcal{F}(\boldsymbol{Q})$ is the collection of the spatial derivatives and the explicit source terms, if any, and $\mathcal{D}(\boldsymbol{Q})$ is artificial dissipation. Thus, $[\mathcal{F}(\boldsymbol{Q}) - \mathcal{D}(\boldsymbol{Q})]$ is the residual. Equation (1) is integrated using the classical (noncompact) four-stage R–K scheme, resulting in fourth-order time accuracy.

Jameson's FAS multigrid pseudo-time-advancing algorithm,[7] however, uses his and his co-workers' compact R–K scheme,[16] which is given as

$$\boldsymbol{Q}^{(0)} = \boldsymbol{Q}^{n} \qquad \boldsymbol{Q}^{(s)} = \boldsymbol{Q}^{n} - \alpha_s J\Delta t\{\mathcal{F}[\boldsymbol{Q}^{(s-1)}] - \mathcal{D}[\boldsymbol{Q}^{(0)}]\} \tag{2}$$

$$\boldsymbol{Q}^{n+1} = \boldsymbol{Q}^{(4)}$$

where the superscript n is the time step, Δt is the time increment from one time step to the next, and $\alpha_s = [\frac{1}{4}, \frac{1}{3}, \frac{1}{2}, 1]$ for $s = 1, 2, 3, 4$, respectively. Here we adopt this scheme directly for the steady-state calculations, because any time-advancing method will not alter the steady-state solution so long as the residual evaluation scheme remains the same. In other words, at the steady state $\mathrm{d}\boldsymbol{Q}/\mathrm{d}t = 0$, leaving the field governed by $\mathcal{F}(\boldsymbol{Q}) - \mathcal{D}(\boldsymbol{Q}) = 0$.

It is useful to introduce the following notation in discussing Jameson's FAS multigrid scheme later. A transfer (restriction) operator for the state variables is denoted by $\mathcal{I}$ and for the residuals by $\mathcal{W}$ and an interpolation (prolongation) operator is denoted by $\mathcal{I}$. All these operators take on subscripts and superscripts that indicate the mesh spacing of the two grids that are involved in the data link, whose direction is understood to be always toward the grid of the superscript. These grids are assumed to be given by the sequence, from the mesh of the desired resolution (h) to the coarsest,

$$G_h,\ G_{2h},\ \ldots,\ G_{rh/2},\ G_{rh},\ \ldots,\ G_{vh} \tag{3}$$

where a subscript indicates the mesh spacing of the grid and r and v are integers that are given by integer powers of 2. Hereafter mesh G_h will sometimes be referred as to the fine mesh.

First the solution on mesh G_{2h} is initialized through the restriction of the data from mesh G_h as

$$\boldsymbol{Q}_{2h}^{(0)} = \mathcal{I}_h^{2h}\boldsymbol{Q}_h \tag{4}$$

where $\boldsymbol{Q}_h$ is the current value of the solution variable on mesh G_h. Then a residual forcing function $\mathcal{P}_{2h}$ is established such that the solution on grid G_{2h} is driven by the residual calculated on grid G_h using the solution $\boldsymbol{Q}_h$. This is achieved by setting

$$\mathcal{P}_{2h} = \mathcal{W}_h^{2h}[\mathcal{F}_h(\boldsymbol{Q}_h) - \mathcal{D}_h(\boldsymbol{Q}_h)] - \{\mathcal{F}_{2h}[\boldsymbol{Q}_{2h}^{(0)}] - \mathcal{D}_{2h}[\boldsymbol{Q}_{2h}^{(0)}]\} \tag{5}$$

This function is added to the residuals in the R–K scheme, which become

$$\boldsymbol{Q}_{2h}^{(s)} = \boldsymbol{Q}_{2h}^{(0)} - \alpha_s(J\Delta t)_{2h}\{\mathcal{F}_{2h}[\boldsymbol{Q}_{2h}^{(s-1)}] - \mathcal{D}_{2h}[\boldsymbol{Q}_{2h}^{(0)}] + \mathcal{P}_{2h}\} \tag{6}$$

Hence, the value of the residual at the first stage will be $\mathcal{W}_h^{2h}[\mathcal{F}_h(\boldsymbol{Q}_h) - \mathcal{D}_h(\boldsymbol{Q}_h)]$ because the other terms will cancel. Thus the solution on grid G_{2h} will be driven by the residual transferred from the fine grid (G_h). It should be noted that the Jacobian and the time increment in the preceding R–K scheme [Eq. (6)] are associated with grid G_{2h}, where the time increment (local) will be significantly larger, consequently a faster propagation of the signals (errors) and an improved convergence rate will result.

The preceding procedure is continued until the coarsest mesh (G_{vh}) is reached, where the correction to the solution will be given by

$$\Delta\boldsymbol{Q}_{vh} = \boldsymbol{Q}_{vh}^{(4)} - \boldsymbol{Q}_{vh}^{(0)} \tag{7}$$

When going back from a coarse grid to the next finer mesh, the accumulated correction is given, on an intermediate grid $G_{rh/2}$, by

$$\Delta\boldsymbol{Q}_{rh/2} = \boldsymbol{Q}_{rh/2}^{\mathrm{new}} - \boldsymbol{Q}_{rh/2} = \mathcal{I}_{rh}^{rh/2}[\boldsymbol{Q}_{rh}^{\mathrm{new}} - \boldsymbol{Q}_{rh}^{(0)}] \tag{8}$$

where $\boldsymbol{Q}_{rh/2}$ is the solution on mesh $G_{rh/2}$ after the R–K time stepping on grid $G_{rh/2}$ and before the interpolation from grid G_{rh}, and $\boldsymbol{Q}_{rh/2}^{\mathrm{new}}$ is the final value of $\boldsymbol{Q}_{rh/2}$ resulting from both the correction calculated in the time step on grid $G_{rh/2}$ and the correction interpolated from grid G_{rh}.

Finally, the updated solution (at time level $n+1$) on the fine grid is given by

$$\boldsymbol{Q}_h^{n+1} = \boldsymbol{Q}_h^{\mathrm{new}} = \boldsymbol{Q}_h + \Delta\boldsymbol{Q}_h \tag{9}$$

The restriction and prolongation operators used to generate the data connections between the grids for the second-order finite difference and finite volume multigrid methods have been established fairly well.[7,10] For example, in finite difference methods, direct injection of the data from a fine grid to the next coarser grid is one practical and extensively used method[10] (Fig. 1). In finite volume methods the transfer of the data is realized through a volume weighted average of four cells on a fine grid that make up one cell of the next coarser grid. This way the flow state variables are conserved.[7] It is very natural to take the volume weighted average of the data in

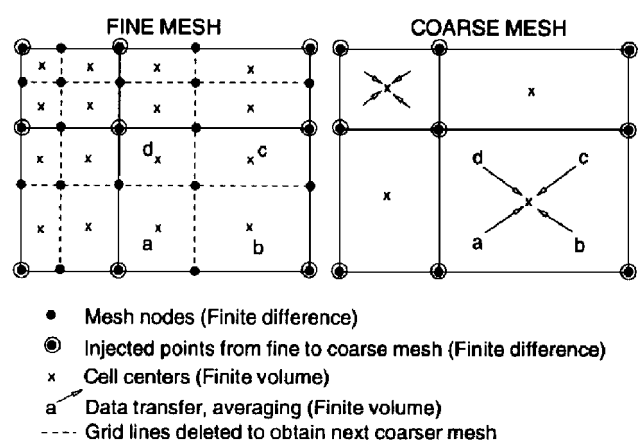

Fig. 1 Data transfer from fine mesh to next coarser mesh in two dimensions.

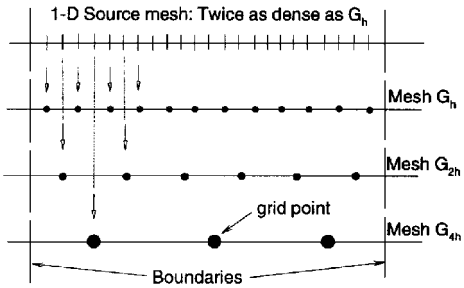

Fig. 2 Obtaining all levels of grid from a source mesh.

finite volume methods because the data are assumed to reside at a cell center, which on the next coarser grid will be affected mostly by the largest of those four constituent cells.

As indicated, the current algorithm uses a fourth-order accurate cell-centered finite difference method, wherein no grid points coincide with the boundaries of the domain. Only in this way does the mesh structure of our current method resemble that of the classical finite volume method. The weighted cell centers in our method, which are the grid points of its finite difference scheme, are not the geometrical cell centers. Instead, they are obtained via high-order interpolations, or the mesh formed by these points is directly produced using the grid generator described in Ref. 3, such that no grid points exist at the solid boundaries. This is important in terms of the smoothness of the geometrical derivatives over the stencils of the finite difference scheme.

For the multigrid application here we generate in each of the ξ, η, and ζ directions (curvilinear coordinate directions) twice as dense a mesh as the fine mesh. We refer to this new mesh as the source mesh, which now has grid lines on the boundaries of the domain. The source mesh readily provides the weighted cell centers or the grid points of the current finite difference method for all the meshes used in the multigrid convergence acceleration process. This point is illustrated, for clarity, in only one dimension, in Fig. 2. Hence, a given mesh level is at least as smooth as the others.

B. Solution and Residual Transfer

In the present approach the transfer operator $\mathcal{I}$ for the dependent variables is defined, in two dimensions, as

$$\boldsymbol{Q}_{2h} = \mathcal{I}_h^{2h}\boldsymbol{Q}_h = \frac{1}{4}\sum_{\text{cell}}^{4}(\boldsymbol{Q}_h)_{\text{cell}} \tag{10}$$

where the four cells that are involved in the summation make up one cell of grid G_{2h}, as illustrated in Fig. 1 for a finite volume method. This simple averaging is preferred over the volume weighted averaging of a finite volume method because of our grid system.

However, the transfer of the residuals is performed along the same lines as Jameson's method. We simply sum the residuals of those four constituent cells on grid G_h to obtain the residual of a G_{2h} cell. Thus for the interior grid points we simply write, for two dimensions,

$$\mathcal{F}_{2h}(\boldsymbol{Q}_{2h}) - \mathcal{D}_{2h}(\boldsymbol{Q}_{2h}) = \mathcal{I}_h^{2h}[\mathcal{F}_h(\boldsymbol{Q}_h) - \mathcal{D}_h(\boldsymbol{Q}_h)]$$
$$= \sum_{\text{cell}}^{4}[\mathcal{F}_h(\boldsymbol{Q}_h) - \mathcal{D}_h(\boldsymbol{Q}_h)]_{\text{cell}} \tag{11}$$

For fully three-dimensional problems, the preceding operations are performed over eight cells for both the residual and solution transfers.

Because the time-accurate calculations use time-dependent nonreflecting BC on the outer boundaries of the domain, steady-state calculations for the engine inlet problems are also performed using the same BC. These conditions are put in the same time-dependent partial differential form as the interior equations (see Ref. 3 or 4). Then the multigrid method is applied to the entire system of equations. The residual transfer operator is, however, defined differently for the far-field boundary points because the solution variables at these points are the perturbed flow quantities. In two dimensions, the residual of a cell on the far-field boundary of the next coarser mesh is taken as two times the sum of the residuals of those constituent cells that correspond to the fine mesh far-field boundary. For three-dimensional problems, this sum is taken over four neighboring cells on the boundary.

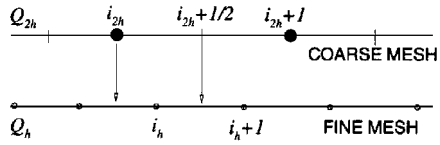

Fig. 3 Grid points involved in prolongation of coarse mesh data to next finer mesh.

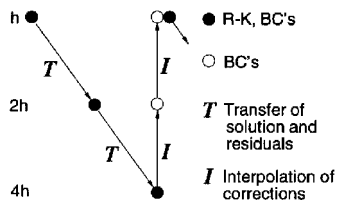

Fig. 4 Three-mesh level sawtooth cycle.

C. Correction Interpolation

The corrections are transferred back to the fine mesh via interpolation. For simplicity, consider the one-dimensional coarse mesh and the next finer mesh shown in Fig. 3. Two finer grid points fall between two coarse grid points. The variation between two coarse grid points is assumed linear and the data at the finer grid points are simply calculated by using the formulas

$$\boldsymbol{Q}_{2h}^{i_{2h}+\frac{1}{2}} = \tfrac{1}{2}(\boldsymbol{Q}_{2h}^{i_{2h}} + \boldsymbol{Q}_{2h}^{i_{2h}+1}) \tag{12}$$

$$\boldsymbol{Q}_h^{i_h} = \mathcal{I}_{2h}^{h}\boldsymbol{Q}_{2h}^{i_{2h},i_{2h}+1} = \tfrac{1}{2}\left(\boldsymbol{Q}_{2h}^{i_{2h}} + \boldsymbol{Q}_{2h}^{i_{2h}+\frac{1}{2}}\right) \tag{13}$$

where a superscript indicates the grid point with which the data are associated (see Fig. 3). Special treatments, such as extrapolation, are needed at or near the boundaries.

D. Cycling Strategy

The so-called sawtooth cycles with three mesh levels are used, although using more grid levels generally improves the efficiency of multigrid methods.[7,10,19] A three-mesh level sawtooth cycle is shown schematically in Fig. 4. The Runge–Kutta time steppings and solution and residual transfers are performed in the direction toward the coarsest mesh, and only correction interpolations are performed in the direction toward the fine mesh. After every restriction of the data from a fine grid to the next coarser grid, the solid wall and the fan-face BC are applied to prevent large jumps that might trigger large adaptive dissipation coefficients. Dissipation is calculated only at the first stage, and its frozen value is used throughout the other stages. Similarly, these BC are also applied after every prolongation operation of the data from a coarse mesh to the next finer mesh. The sawtooth cycles are started on the fine mesh (G_h) from the first step of the pseudotime advancement and continued until convergence is obtained.

IV. Results and Discussion

The current method has been implemented on CM-5 using the data parallel paradigm and has been shown to calculate steady-state flows around various geometries effectively, including transonic flows around airfoils.[20] In this paper, results relating to a turbofan engine inlet are presented, and it is demonstrated that the current fourth-order multigrid method is an important component in the present engine inlet noise prediction methodology.

In multigrid work the root mean square (rms) residual or the error is usually plotted vs the number of work units so that the convergence rates can be compared in the same norms with those given by using single meshes. This is because one has to perform more operations in a multigrid cycle than in a single mesh cycle (equivalent to one time

step or iteration for single mesh). The total number of operations is usually proportional to

$$C = \left[c_0 + \sum_{\text{levels}} \left(\frac{1}{2} \right)^{N(q-1)} \right]$$

for a sawtooth cycle, where c_0 is the overhead factor, the sum is due to performing calculations on multiple grids, and N is the number of dimensions in which the problem is being solved. The overhead is usually caused by the restriction and prolongation operations as well as the application of the solid wall and the fan-face BC after each of the transfer operations. The total cost factor C for the present code is about 1.8. This factor includes the overhead associated with the programming strategy as well. Therefore, the ratio of the multigrid convergence to single mesh convergence per fine mesh iteration must be over at least 1.8 so that one can talk about convergence improvement using the multigrid method. In other words, the convergence improvement per time step using the multigrid method must not be offset by the introduced overhead and the increase in the number of operations. One good measure would be the convergence rate given per CPU time. However, the CPU time is usually machine dependent. Therefore, we present the results showing the convergence vs the number of fine mesh iterations curve.

A. Steady Flow Around JT15D Inlet

Results presented in this section and the next pertain to the JT15D inlet geometry[21] (without a centerbody) at zero angle of attack. Figure 5 illustrates the inlet geometry together with the mesh topology[3] used and the locations of two typical example Kirchhoff surfaces. The Kirchhoff surfaces are used in the far-field noise computations.[2,3] All mesh levels used in the multigrid solution process are generated using conformal mapping as indicated earlier. The far-field boundaries are placed as close as only 1.5–2.0 inlet diameters from the inlet lip. At the fan, one-dimensional characteristic based, nonreflecting BC are used.[3,22]

Figure 6 compares the convergence histories (normalized density residual) of the single mesh and multigrid runs for a freestream Mach number of 0.204 and a mass flow rate (MFR) of 14 kg/s. The fine

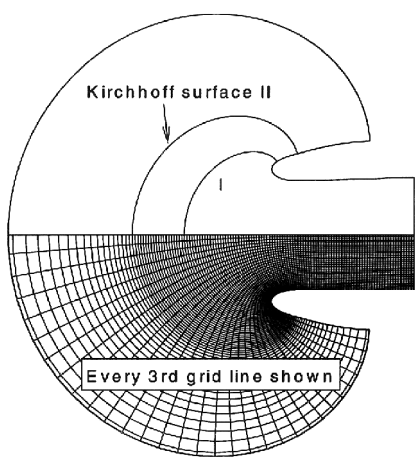

Fig. 5 Mesh system (384 × 96 × 1) and two typical Kirchhoff surfaces around the JT15D inlet.

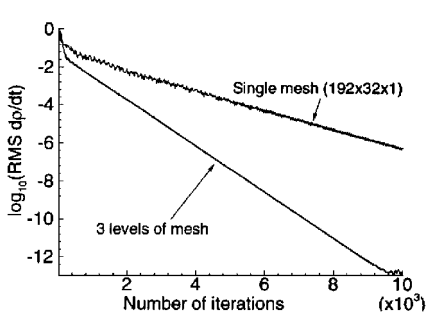

Fig. 6 Convergence history of the steady-state problem on the fine mesh (192 × 32 × 1): JT15D inlet, $M_\infty = 0.204$, $\alpha = 0$ deg, and MFR = 14 kg/s.

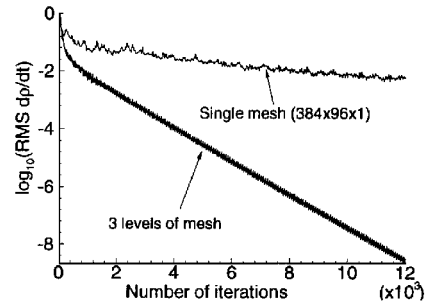

Fig. 7 Convergence history of the steady-state problem on the fine mesh (384 × 96 × 1): JT15D inlet, $M_\infty = 0.192$, $\alpha = 0$ deg, and MFR = 22 kg/s.

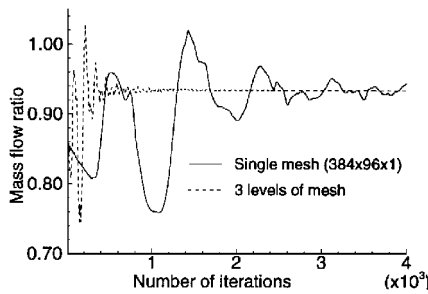

Fig. 8 Convergence in terms of the mass flow ratio on the fine mesh (384 × 96 × 1): JT15D inlet, $M_\infty = 0.192$, $\alpha = 0$ deg, and MFR = 22 kg/s.

mesh for this case had 192 × 32 × 1 cells with aspect ratios varying from nearly 1 to 5. A significant improvement in convergence per time step using the multigrid method is evident.

It is extremely important to drive the numerical errors to very low levels so that they do not contaminate the acoustic solutions. Therefore, in noise prediction calculations, the steady-state flow residual is usually driven about 10 orders of magnitude down from its initial value. It has been experienced that single-grid runs do not usually yield such residual reductions at a constant rate. Sometimes the solution does not converge at all to these levels. This is illustrated in Fig. 7, where the convergence histories are shown for $M_\infty = 0.192$ and MFR = 22 kg/s. This operating condition corresponds to a higher fan speed (rpm), which in turn results in a higher-frequency acoustic field. Therefore, a finer mesh is needed for acoustic response calculations. Thus for this second example a mesh of 384 × 96 × 1 cells was used. This mesh is shown in Fig. 5. It is extremely difficult to attain a steady-state flowfield in a reasonable number of time steps on such fine meshes using the fourth-order accurate algorithm, as indicated by the single grid convergence curve (Fig. 7). However, using the FAS multigrid technique, we observed a significant improvement. It is evident by comparing Figs. 6 and 7 that the improvement rate tends to increase as the mesh is further refined. This can be attributed to the increase in the transferred error bandwidth during the restriction and prolongation operations.

Through multigrid iterations the residual is expelled more quickly out of the domain as mentioned earlier. Another good measure that shows this is the mass flow ratio history, which is shown in Fig. 8 for the second case. Mass flow ratio is defined as the ratio of the captured freestream tube area to the inlet cross section at the inlet leading edge. It is evident that the mass flow ratio with the multigrid method approached the specified mass flow ratio, which is fixed by the specified mass flow rate, and stabilized within only 1000 time steps, whereas it did not at all for the single grid. This behavior of multigrid methods is crucial in rapid aerodynamic design analyses.[19] The one-dimensional characteristic fan-face BC implementation described by Özyörük[3] yielded an extremely accurate mass flow ratio at convergence to steady state. The computed mass flow ratio is 0.935 as compared with the specified 0.938. The error is well below 1%.

The steady flowfield Mach number contours for the second case are shown in Fig. 9. It is clear that the flow accelerates in the throat region due to the high mass flow rate. The Mach number in this region reaches 0.27. This means that the wavelength of the acoustic waves in the upstream direction is shortened by a factor of 0.73(= 1.0 − M). This is a disadvantage in the ducted fan noise

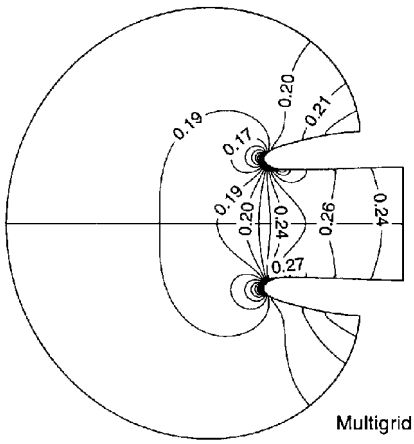

Fig. 9 Mach contours at the steady state: JT15D inlet, $M_\infty = 0.192$, $\alpha = 0$ deg, and MFR = 22 kg/s.

computations. Notice that the contour lines are extremely smooth across the centerline, showing no signs of significant numerical errors due to the mesh singularity. One has to be careful with the treatment[3,4] of this boundary not to contaminate the acoustic waves with numerical errors.

B. Acoustic Radiation from JT15D Inlet

The goal of this section is to illustrate how well the present approach of the determination of the acoustic field by the subtraction of the multigrid steady solution from the time-accurate solution works. For this, the acoustic field of a spinning mode of a JT15D test engine is predicted at actual flight conditions. The JT15D engine test configuration has an array of 41 rods placed in front of the 28-blade rotor, which produces mode (13, 0) interaction tones at the BPF.[21,23] The (13, 0) mode corresponds to fan loadings concentrated toward the blade tips as indicated by the source model.[2] Therefore, the unsteady field is expected to develop near the wall in the engine inlet and then radiate to the far field.

Two cases are presented here. In the first case the engine inlet carries a mass flow of 17.297 kg/s at the flight Mach number $M_\infty = 0.204$ with an engine speed of 8120 rpm and in the second case a mass flow of 19.275 kg/s at $M_\infty = 0.2$ with 9343 rpm. The (13, 0) mode at these conditions has BPFs of 3789.3 and 4360 Hz, respectively. These frequencies correspond, in order, to the dimensionless frequency parameters $[(kr)_f]$ 18.65 and 21.48, where k_f is the wave number and r_f the duct radius at the fan stage.

The steady-state part of the problem was solved on an axisymmetric, $384 \times 96 \times 1$ mesh through the present multigrid method for both cases. This mesh is the same as the one used in the previous section and is shown in Fig. 5. The steady-state solution was then spread out onto one of the 13 periodic three-dimensional grids to start the time-accurate part of the solution, using periodic BC in the circumferential direction. One, in fact, does not need to solve this problem on a fully 360-deg mesh because a single spinning mode generates periodic pressure patterns in the azimuthal direction. The (13, 0) mode generates periodic patterns at every 360/13 deg. Therefore, the time-accurate solution was obtained on a $384 \times 96 \times 16$ mesh, having 16 cells per circumferential lobe.

A snapshot of the acoustic pressure contours in the inlet is shown in Fig. 10, where the rms acoustic pressure contours are also shown. The directivity trend of the radiating (13, 0) mode is evident from the figure. It is clear that the acoustic pattern is well defined in the vicinity of the engine inlet wall, as expected. Other regions are silent in the inlet. This means that the unsteady solution process preserved the steady solution that was obtained through the present multigrid method perfectly where acoustic effects were absent.

For the second case only the Kirchhoff results are presented. The location of the Kirchhoff surface used for the calculations is shown in Fig. 10. The far-field sound pressure levels (SPL) as calculated for 24 observer points at a distance of 30.48 m at every 3 deg are shown in Fig. 11 along with the experimental data[23] and the finite element wave envelope (FE-WE) solution of Eversman et al.[23] These

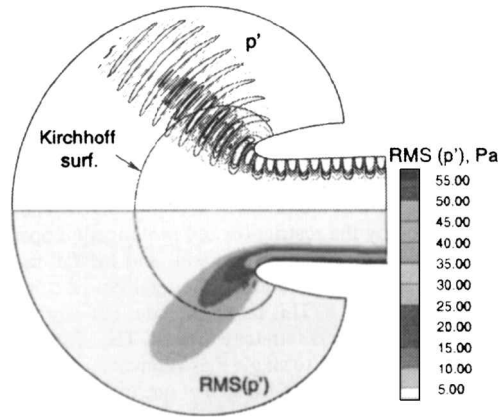

Fig. 10 Instantaneous and rms acoustic pressure contours and the Kirchhoff surface location of the (13, 0) mode: JT15D inlet, $M_\infty = 0.204$, MFR = 17.297 kg/s, BPF = 3789.3 Hz, and $(kr)_f = 18.65$.

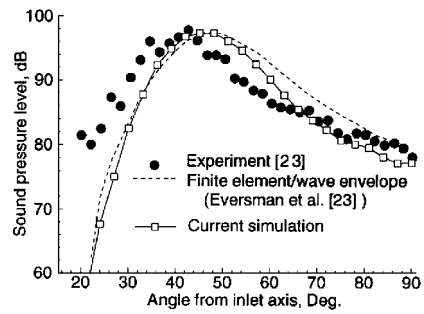

Fig. 11 Far-field sound pressure level of the (13, 0) mode: JT15D inlet, $M_\infty = 0.2$, MFR = 19.295 kg/s, BPF = 4360 Hz, and $(kr)_f = 21.48$.

results were all scaled to have a peak SPL of 100 dB. The Kirchhoff integrations were carried out at every 12th R–K iteration. The comparison of the current simulation with the experimental data reveals very good agreement in general, although the prediction has the SPL peak at a somewhat higher angle from the negative x axis. Similar difference is observed between the FE-WE solution and experiment. However, the current simulation has about a 2-deg better prediction of the peak SPL angle than the FE-WE method. The reason for the differences between the experiment and the numerical simulations can be attributed to the experimental data reduction as well as the source models of the methods representing the actual source, namely the rotor–stator interactions, only approximately. Nonetheless, the source has been modeled reasonably well.

V. Conclusions

Convergence acceleration is essential in the ducted fan noise prediction methods solving the full, time-dependent Euler equations together with nonreflecting BC. For this purpose, a multigrid convergence acceleration technique that retains the high-order accuracy of a typical, explicit, high-resolution CAA algorithm has been developed and implemented on CM-5 in a data parallel fashion using CM Fortran. Particularly, Jameson's full approximation storage method has been utilized. The method has been applied successfully both to the time-dependent Euler and nonreflecting BC equations. Although only three-mesh levels with sawtooth cycles have been used, the improved convergence characteristics of the hybrid code with the multigrid method have made it possible to attain steady-state flows at low Mach numbers on very fine grids. This in turn makes high-frequency acoustic predictions viable through the present approach. Steady-state flow and far-field noise simulations have been presented for an actual turbofan engine inlet, and comparisons with flight data and other numerical results have indicated very good agreement.

Acknowledgments

This work was supported by the NASA Langley Research Center under Grant NAG-1-1367. Computational resources (CM-5) were

provided by the National Center for Supercomputing Applications at the University of Illinois at Urbana–Champaign.

References

[1]Chyczewski, T. S., and Long, L. N., "Numerical Prediction of the Noise Produced by a Perfectly Expanded Rectangular Jet," AIAA Paper 96-1730, May 1996.

[2]Özyörük, Y., and Long, L. N., "Computation of Sound Radiating from Engine Inlets," *AIAA Journal*, Vol. 34, No. 5, 1996, pp. 894–901.

[3]Özyörük, Y., "Sound Radiation from Ducted Fans Using Computational Aeroacoustics on Parallel Computers," Ph.D. Thesis, Dept. of Aerospace Engineering, Pennsylvania State Univ., University Park, PA, Dec. 1995.

[4]Özyörük, Y., and Long, L. N., "A New Efficient Algorithm for Computational Aeroacoustics on Parallel Processors," *Journal of Computational Physics*, Vol. 125, No. 1, 1996, pp. 135–149.

[5]Farassat, F., and Myers, M. K., "Extension of Kirchhoff's Formula for Radiation from Moving Surfaces," *Journal of Sound and Vibration*, Vol. 123, No. 3, 1988, pp. 451–460.

[6]Bangalore, A., Morris, P. J., and Long, L. N., "A Parallel Three-Dimensional Computational Aeroacoustics Method Using Non-Linear Disturbance Equations," AIAA Paper 96-1728, May 1996.

[7]Jameson, A., "Multigrid Algorithms for Compressible Flow Calculations," *Multigrid Methods II, Proceedings of the 2nd European Conference on Multigrid Methods*, No. 1228, Lecture Notes in Mathematics, Springer–Verlag, New York, 1986, pp. 166–201.

[8]Chima, R. V., and Johnson, G. M., "Efficient Solution of the Euler and Navier–Stokes Equations with a Vectorized Multiple-Grid Algorithm," AIAA Paper 83-1893, July 1983.

[9]Ni, R.-H., "A Multiple-Grid Scheme for Solving the Euler Equations," *AIAA Journal*, Vol. 20, No. 11, 1982, pp. 1565–1571.

[10]Chima, R. V., Turkel, E., and Schaffer, S., "Comparison of Three Explicit Multigrid Methods for the Euler and Navier–Stokes Equations," AIAA Paper 87-0602, Jan. 1987.

[11]Agarwal, R. K., "Unigrid and Multigrid Algorithms for the Solution of Coupled, Partial-Differential Equations Using Fourth-Order-Accurate Compact Differencing," Symposium on Numerical Boundary Conditions Procedures and Multigrid Methods, MDRL 81-35, NASA Ames Research Center, Moffett Field, CA, Oct. 1981.

[12]Liu, C., and Liu, Z., "High Order Finite Difference and Multigrid Methods for Spatially Evolving Instability in a Planar Channel," *Journal of Computational Physics*, Vol. 106, No. 1, 1993, pp. 92–100.

[13]Bayliss, A., and Turkel, E., "Far Field Boundary Conditions for Compressible Flow," *Journal of Computational Physics*, Vol. 48, Nov. 1982, pp. 182–199.

[14]Tam, C. K. W., and Webb, J. C., "Dispersion-Relation-Preserving Finite Difference Schemes for Computational Acoustics," *Journal of Computational Physics*, Vol. 107, No. 2, 1993, pp. 262–281.

[15]Ives, D. C., and Menor, W. A., "Grid Generation for Inlet-Centerbody Configurations Using Conformal Mapping and Stretching," AIAA Paper 81-0997, June 1981.

[16]Jameson, A., Schmidt, W., and Turkel, E., "Numerical Solutions of the Euler Equations by Finite Volume Methods Using Runge–Kutta Time-Stepping Schemes," AIAA Paper 81-1259, June 1981.

[17]Swanson, R. C., and Turkel, E., "Artificial Dissipation and Central Difference Schemes for the Euler and Navier–Stokes Equations," AIAA Paper 87-1107, June 1987.

[18]Tyler, J. M., and Sofrin, T. G., "Axial Flow Compressor Noise Studies," *SAE Transactions*, Vol. 70, 1962, pp. 309–332.

[19]Jameson, A., "Successes and Challenges in Computational Aerodynamics," AIAA Paper 87-1184, June 1987.

[20]Özyörük, Y., and Long, L. N., "Progress in Time-Domain Calculations of Ducted Fan Noise: Multigrid Acceleration of a High-Resolution CAA Scheme," AIAA Paper 96-1771, May 1996.

[21]Preisser, J. S., Silcox, R. J., Eversman, W., and Parret, A. V., "A Flight Study of Tone Radiation Patterns Generated by Inlet Rods in a Small Turbofan Engine," AIAA Paper 84-0499, Jan. 1984.

[22]Giles, M. B., "Nonreflecting Boundary Conditions for Euler Equation Calculations," *AIAA Journal*, Vol. 28, No. 12, 1990, pp. 2050–2058.

[23]Eversman, W., Parret, A. V., Preisser, J. S., and Silcox, R. J., "Contributions to the Finite Element Solution of the Fan Noise Radiation Problem," *Transactions of the American Society of Mechanical Engineers*, Vol. 107, April 1985, pp. 216–223.

S. Glegg
Associate Editor